

Quantifying the Consequences of the Ill-Defined Nature of Neutral Surfaces

ANDREAS KLOCKER*

*CSIRO Marine and Atmospheric Research, and Antarctic Climate and Ecosystems Cooperative Research Center,
and Institute of Antarctic and Southern Ocean Studies, University of Tasmania, Hobart, Tasmania, Australia*

TREVOR J. MCDUGALL

*Centre for Australian Climate and Weather Research, CSIRO and Bureau of Meteorology,
Hobart, Tasmania, Australia*

(Manuscript received 5 January 2009, in final form 1 December 2009)

ABSTRACT

In the absence of diapycnal mixing processes, fluid parcels move in directions along which they do not encounter buoyant forces. These directions define the local neutral tangent plane. Because of the nonlinear nature of the equation of state of seawater, these neutral tangent planes cannot be connected globally to form a well-defined surface in three-dimensional space; that is, continuous “neutral surfaces” do not exist. This inability to form well-defined neutral surfaces implies that neutral trajectories are helical. Consequently, even in the absence of diapycnal mixing processes, fluid trajectories penetrate through any “density” surface. This process amounts to an extra mechanism that achieves mean vertical advection through any continuous surface such as surfaces of constant potential density or neutral density. That is, the helical nature of neutral trajectories causes this additional diasurface velocity. A water-mass analysis performed with respect to continuous density surfaces will have part of its diapycnal advection due to this diasurface advection process. Hence, this additional diasurface advection should be accounted for when attributing observed water-mass changes to mixing processes. Here, the authors quantify this component of the total diasurface velocity and show that locally it can be the same order of magnitude as diasurface velocities produced by other mixing processes, particularly in the Southern Ocean. The magnitude of this diasurface advection is proportional to the ocean’s neutral helicity, which is observed to be quite small in today’s ocean. The authors also use a perturbation experiment to show that the ocean rapidly readjusts to its present state of small neutral helicity, even if perturbed significantly. Additionally, the authors show how seasonal (rather than spatial) changes in the ocean’s hydrography can generate a similar vertical advection process. This process is described here for the first time; although the vertical advection due to this process is small, it helps to understand water-mass transformation on density surfaces.

1. Introduction

Diapycnal mixing in the deep ocean is a key process by which dense water that sinks near the poles is made less dense and returned to the sea surface as part of the thermohaline circulation. However, in addition to the diapycnal motion that is caused by diapycnal mixing, there are several other physical processes that can cause

diapycnal motion. Double-diffusive convection is perhaps the best known of these additional processes. In addition, there is the diapycnal motion caused by cabbeling and thermobaricity, with both being caused by a combination of isopycnal mixing and the nonlinear nature of the equation of state. Neither cabbeling nor thermobaricity has a signature in the dissipation of mechanical energy; that is, both cabbeling and thermobaricity operate independently of the amount of diapycnal mixing.

There are (at least) three other processes by which seawater can migrate through isopycnals without the need for diapycnal mixing. First, submesoscale coherent vortices, by maintaining anomalous water-mass characteristics, are able to migrate through density surfaces (McDougall 1987c). This process is essentially a finite amplitude version of thermobaricity. The second and

* Current affiliation: Massachusetts Institute of Technology, Cambridge, Massachusetts.

Corresponding author address: Andreas Klocker, Massachusetts Institute of Technology, 77 Massachusetts Ave., Cambridge, MA 02139.
E-mail: aklocker@mit.edu

third processes are the subject of the present paper: the second is the mean vertical motion achieved by the ocean circulation because of the helical nature of neutral trajectories in space, and the third is a temporal analog of this neutral helical advection. This third temporal helical motion is described in this paper for the first time. In the remainder of this introduction, we discuss the previous work that has appeared in the literature on the spatial neutral helical advection process.

Reid and Lynn (1971) were the first to discuss the possibility of neutral surfaces being ill defined. They showed that lateral mixing along a locally referenced potential density surface at one pressure, followed by a pressure excursion and then isopycnal mixing at the new pressure, and finally a subsequent movement back to the original pressure results in a difference in the potential density at the original pressure. In this way, they showed that a neutral trajectory could be helical in nature. The example discussed by Reid and Lynn (1971) did not come from the real ocean, and the authors thought that this process would not be important in the real ocean. Ivers (1975) discussed the same process but thought (incorrectly) that such helical motion could only occur if the water column had neutral vertical stability (i.e., zero buoyancy frequency) somewhere. McDougall and Jackett (1988) introduced theoretical relationships between the pitch of the neutral helix and the nature of the thermodynamic variables in space, introducing the concept of neutral helicity. The concept introduced by Reid and Lynn (1971) of isopycnal mixing at two distinctly different pressures is the physical process that underlies the theory developed by McDougall and Jackett [1988; see Fig. 1a of McDougall and Jackett (1988) for a sketch of the concept introduced by Reid and Lynn (1971)]. Theodorou (1991) has analyzed data from the Mediterranean and from the northern North Atlantic to quantify the vertical pitch of the neutral helix in these locations, finding the vertical ambiguity to be no more than 4 m.

2. Consequences of neutral helicity

It is known that, in the absence of diapycnal mixing processes, a fluid moves along the neutral tangent plane (McDougall 1987a; McDougall and Jackett 1988). Locally, we can define these neutral tangent planes (i.e., the direction along which a fluid parcel can move without working against buoyancy forces; McDougall 1987a); however, because of the helical nature of neutral trajectories, these neutral tangent planes cannot be connected globally to form a continuous “density” surface. Therefore, density surfaces such as potential density surfaces or approximately neutral surfaces are only approximations to the directions along which fluid parcels

move. When discussing continuous “density” surfaces, we therefore put density into quotes to remind that we are talking about surfaces along which a certain density variable (such as potential density or neutral density) is constant, even though water parcels following these surfaces do have to do work against buoyant restoring forces. It has been shown that the error between a continuous “density” surface and the neutral tangent planes can be reduced substantially by using appropriate techniques (Jackett and McDougall 1997; Klocker et al. 2009a,b; D. R. Jackett et al. 2009, unpublished manuscript), but it is impossible to define a surface that has a slope equal to the neutral tangent plane at every point. Such a surface would only be possible if neutral helicity in the ocean, defined as

$$H^n \equiv (\alpha^\Theta \nabla \Theta - \beta^\Theta \nabla S) \cdot \nabla \times (\alpha^\Theta \nabla \Theta - \beta^\Theta \nabla S), \quad (1)$$

is everywhere zero (McDougall and Jackett 1988). Here, $\alpha^\Theta \nabla \Theta - \beta^\Theta \nabla S$ is normal to the local direction of mixing (i.e., the neutral tangent plane), where α^Θ is the thermal expansion coefficient and β^Θ is the saline contraction coefficient with respect to conservative temperature Θ . Neutral helicity can also be written as any of the following three expressions (McDougall and Jackett 2007):

$$\begin{aligned} H^n &= \beta^\Theta T_b^\Theta \nabla p \cdot \nabla S \times \nabla \Theta, \\ &= p_z \beta^\Theta T_b^\Theta \nabla_p S \times \nabla_p \Theta \cdot \mathbf{k}, \\ &= g^{-1} N^2 T_b^\Theta \nabla_n p \times \nabla_n \Theta \cdot \mathbf{k}, \\ &\approx g^{-1} N^2 T_b^\Theta \nabla_a p \times \nabla_a \Theta \cdot \mathbf{k}, \end{aligned} \quad (2)$$

where T_b^Θ is the thermobaric parameter,

$$T_b^\Theta = \beta^\Theta (\alpha^\Theta / \beta^\Theta)_p. \quad (3)$$

Here, ∇_a is the gradient along an approximately neutral surface. The derivation of Eq. (2) can be found in McDougall and Jackett (1988, 2007). The last line of Eq. (2) is an approximation to neutral helicity. It would be an exact identity if the gradients of pressure and temperature in the approximately neutral surface were equal to those in the neutral tangent plane, $\nabla_n p$ and $\nabla_n \Theta$. In most regions, the ocean seems to adjust itself so that neutral helicity is close to zero, as demonstrated in McDougall and Jackett (2007). However, as long as neutral helicity is not exactly equal to zero, a mathematically well-defined density surface does not describe the direction of lateral mixing. Because of this resulting slope error, there is a fictitious diapycnal diffusivity of density (Klocker et al. 2009a) and an additional diapycnal advection through any continuous “density” surface.

The diapycnal advection through continuous “density” surfaces can be derived in terms of the diapycnal

velocity through neutral tangent planes by the following argument: First, we note the conservation equations for salinity and conservative temperature,

$$S_t|_n + \mathbf{V} \cdot \nabla_n S + e S_z = h^{-1} \nabla_n \cdot (hK \nabla_n S) + (DS_z)_z \quad \text{and} \quad (4)$$

$$\Theta_t|_n + \mathbf{V} \cdot \nabla_n \Theta + e \Theta_z = h^{-1} \nabla_n \cdot (hK \nabla_n \Theta) + (D\Theta_z)_z, \quad (5)$$

where ∇_n is the gradient operator in the neutral tangent plane; \mathbf{V} is the thickness-weighted lateral velocity, averaged between a pair of closely spaced neutral tangent planes whose average vertical separation is h ; and S and Θ are the thickness-weighted salinity and conservative temperature. An expression for the diapycnal velocity e through neutral tangent planes is obtained in terms of mixing processes by cross multiplying Eqs. (4) and (5) by β^Θ and α^Θ , respectively, and then subtracting to find

$$\begin{aligned} e \frac{N^2}{g} &= \alpha^\Theta (D\Theta_z) - \beta^\Theta (DS_z) + h^{-1} \alpha^\Theta \nabla_n \cdot (hK \nabla_n \Theta) - h^{-1} \beta^\Theta \nabla_n \cdot (hK \nabla_n S), \\ &= \alpha^\Theta (D\Theta_z) - \beta^\Theta (DS_z) - KC_b^\Theta \nabla_n \Theta \cdot \nabla_n \Theta - KT_b^\Theta \nabla_n \Theta \cdot \nabla_n p, \end{aligned} \quad (6)$$

where C_b^Θ and T_b^Θ are the cabbeling and thermobaric coefficients defined in McDougall (1987b) and Klocker and McDougall (2010).

The right-hand side (rhs) of Eq. (6) describes small-scale turbulent mixing (the first two terms) and processes due to the nonlinear equation of state (the third and fourth terms): namely, cabbeling and thermobaricity. These terms on the right-hand side of Eq. (6) are explained in detail in Klocker and McDougall (2010) and will not be discussed here.

We now write the material derivative of S and Θ on the left-hand side of Eqs. (4) and (5) with respect to continuous “density” surfaces so that they become

$$S_t|_a + \mathbf{V} \cdot \nabla_a S + e^a S_z = h^{-1} \nabla_n \cdot (hK \nabla_n S) + (DS_z)_z \quad \text{and} \quad (7)$$

$$\Theta_t|_a + \mathbf{V} \cdot \nabla_a \Theta + e^a \Theta_z = h^{-1} \nabla_n \cdot (hK \nabla_n \Theta) + (D\Theta_z)_z. \quad (8)$$

Here, e^a is the vertical velocity through the continuous approximately neutral surface (or any other continuous “density” surface), and \mathbf{V} is now the thickness-weighted lateral velocity averaged between a pair of closely spaced approximately neutral surfaces. These equations are again cross multiplied by the same β^Θ and α^Θ coefficients and subtracted, obtaining [using Eq. (6)]

$$\begin{aligned} e^a &= e + \frac{g}{N^2} \mathbf{V} \cdot (\beta^\Theta \nabla_a S - \alpha^\Theta \nabla_a \Theta) \\ &\quad + \frac{g}{N^2} (\beta^\Theta S_t|_a - \alpha^\Theta \Theta_t|_a). \end{aligned} \quad (9)$$

From Klocker et al. (2009a) we know that

$$\frac{g}{N^2} (\beta^\Theta \nabla_a S - \alpha^\Theta \nabla_a \Theta) = \nabla_n z - \nabla_a z = \mathbf{s}; \quad (10)$$

that is, \mathbf{s} is the vector slope difference between the slope of a neutral tangent plane and the slope of the approximately neutral surface (or any other continuous “density” surface). Hence, the middle term on the right-hand side of Eq. (9), $\mathbf{V} \cdot \mathbf{s}$, is the vertical velocity through the approximately neutral surface due to the lateral flow occurring along the neutral tangent plane. Because of the slope error \mathbf{s} , this vertical velocity through approximately neutral surfaces depends on the surface used. When the approximately neutral surface is formed very accurately, such as the ω surfaces by Klocker et al. (2009a), $\mathbf{V} \cdot \mathbf{s}$ is almost solely due to neutral helicity,¹ and we label $\mathbf{V} \cdot \mathbf{s}$ as e^{hel} , the vertical velocity through the ω surface due to neutral helicity.

The term e^{hel} can be understood by looking at Fig. 1. In this figure, the blue surface is an approximately neutral surface γ^a , the red arrow describes a fluid trajectory (which in the absence of mixing processes is along local neutral tangent planes) with lateral velocity \mathbf{V} , and φ ($\tan \varphi = |\mathbf{s}|$) is the angle between the approximately neutral surface and the fluid trajectory. Note that, if Eq. (9) is used in a neutral tangent plane, the slope error [Eq. (10)] would equal zero, leading to $e^{\text{hel}} = 0$. This shows that it is necessary to take this diapycnal advection due to neutral helicity e^{hel} into account when using continuous “density” surfaces for water-mass analysis (where $\mathbf{s} \neq 0$) but

¹ Because of the way the algorithm by Klocker et al. (2009a) works, we know that in an ocean with zero neutral helicity this algorithm will find a surface on which the slope error \mathbf{s} is zero. However, by using different weights when solving the set of equations by the direct inversion or the iterative technique, this algorithm would result in a slightly different ω surface in an ocean with nonzero neutral helicity. Nevertheless, in the case of an ocean with zero neutral helicity, all choices of weight would lead to a surface with zero slope error.

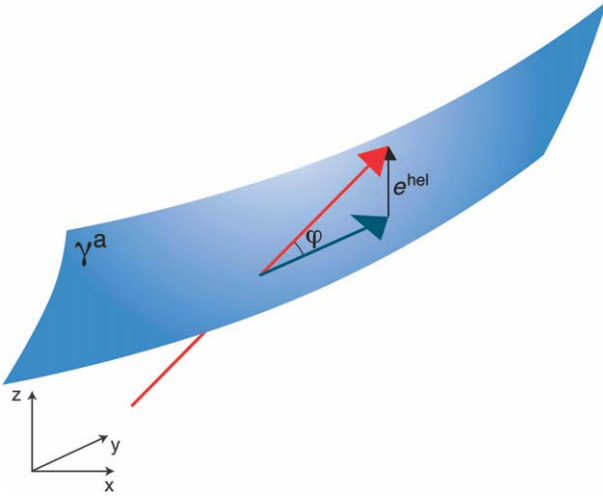


FIG. 1. Schematic of the diapycnal velocity e^{hel} due to neutral helicity. Here, we ignore all other diapycnal processes, such as cabbeling, thermobaricity, and small-scale turbulent mixing. The blue surface shows an approximately neutral surface (a γ^a surface); the red arrow shows the path of a fluid trajectory (which is along the neutral tangent plane) with lateral velocity \mathbf{V} ; φ ($\tan \varphi \approx |\mathbf{s}|$) is the angle between the γ^a surface and the neutral tangent plane; and e^{hel} is the diapycnal velocity due to neutral helicity $\mathbf{V} \cdot \mathbf{s}$.

not when doing this water-mass analysis locally with respect to a neutral tangent plane (where $\mathbf{s} = 0$).

Similarly, the last term in Eq. (9) can be written as

$$\frac{g}{N^2}(\beta^\Theta S_t|_a - \alpha^\Theta \Theta_t|_a) = \frac{-\rho_t|_a}{\rho_z} = z_t|_n - z_t|_a, \quad (11)$$

namely, the vertical velocity of the neutral tangent plane (at fixed latitude and longitude) minus the vertical velocity of the approximately neutral surface, with ρ' being the locally referenced potential density. This is then the vertical velocity through the approximately neutral surface due to water parcels simply moving vertically while staying on the neutral tangent plane (in time at fixed x and y). In section 5 of this paper, we call this vertical velocity [Eq. (11)], which is described in this work for the first time e^{tmp} .

Rewriting Eq. (9), we can express the vertical velocity through an approximately neutral surface e^a as

$$\begin{aligned} e^a &= e + \mathbf{V} \cdot (\nabla_n z - \nabla_a z) + z_t|_n - z_t|_a, \\ &= e + e^{\text{hel}} + e^{\text{tmp}}. \end{aligned} \quad (12)$$

Note that the words “diapycnal” and “isopycnal” are generally used to describe diasurface and along-surface flow as well as flow through and along a neutral tangent plane. To be more accurate about which directions are meant when using the terms diapycnal and isopycnal, we

recommend the use of the symbol e for the diapycnal velocity through a neutral tangent plane and e^a for the diapycnal flow through a well-defined (i.e., continuous) “density” surface, which we frequently call an approximately neutral surface.

The aim of this paper is to quantify the diapycnal velocities attributable to neutral helicity. We will show that in some regions these diapycnal velocities are of the same order of magnitude as those caused by the usual water-mass transformation processes. This is particularly true for the Southern Ocean, where these “extra” diapycnal velocities need to be taken into account when analyzing water-mass transformation on continuous “density” surfaces. To quantify these diapycnal velocities, we calculate e^{hel} at every point on a surface and sum the diapycnal transport from these velocities (an Eulerian perspective). An alternative method (McDougall and Jackett 1988) is to follow neutral trajectories in the ocean to calculate their vertical excursion from an approximately neutral surface (a Lagrangian perspective). The latter method is based on two assumptions that are hard to justify in the ocean (discussed in the appendix), and therefore we do not use this approach here. A more sophisticated Lagrangian approach would be to use full Lagrangian particle trajectories of millions of parcels in an ocean model.

We note that, in calculating the diapycnal velocities attributable to the slope error, \mathbf{s} in Eq. (10) does not have to be caused by neutral helicity but can be a result of the definition of the continuous “density” surface used. We will demonstrate how e^{hel} can change when using different continuous “density” surfaces by comparing diapycnal velocities through accurate approximately neutral surfaces [e.g., the γ^n surfaces by Jackett and McDougall (1997) or the ω surfaces by Klocker et al. (2009a,b)] with those through potential density surfaces. To distinguish e^{hel} through these various surfaces, we will use the symbols e_ω^{hel} , $e_{\gamma^n}^{\text{hel}}$, $e_{\sigma_\theta}^{\text{hel}}$, etc. for e^{hel} through ω surfaces, γ^n surfaces, and σ_θ surfaces, respectively.

The estimates of the diapycnal velocities e^{hel} through the best type of approximately neutral surfaces depend on the magnitude of neutral helicity in the ocean. From McDougall and Jackett (2007), we know that the ocean is in a state in which neutral helicity is relatively small but nonzero. Therefore, we conduct an experiment in which we push the ocean into a state in which neutral helicity is significantly larger than in its normal state. This experiment helps to understand if or how the ocean adjusts back to its normal state and how this perturbation affects the diapycnal velocity e^{hel} .

We will also show how temporal changes in the ocean’s hydrography can cause vertical advection e^{tmp} because of these same nonlinear effects. The idea behind this process is similar to the diapycnal advection

due to neutral helicity, as described earlier; however, instead of being dependent on the spatial variation of S , Θ , and p , this vertical advection is due to seasonal changes of the ocean's hydrography.

3. Quantifying diapycnal advection through continuous “density” surfaces

To quantify the diapycnal advection due to neutral helicity, we need a dataset with salinity, temperature, pressure, and lateral velocity. Because of the sparseness of velocity measurements in the ocean, we have to use model output for this analysis. The model we use here is version 4 of the Modular Ocean Model (MOM4; Griffies et al. 2004). The standard MOM4 configuration is used, but with conservative temperature (McDougall 2003) instead of potential temperature as the model's conserved temperature variable, although this change is not important for the results in this paper. This model configuration uses an isopycnal diffusivity of $1000 \text{ m}^2 \text{ s}^{-1}$, the vertical mixing scheme by Bryan and Lewis (1979), and the McDougall et al. (2003) equation of state. The “density” surfaces we use here to compute e_{ω}^{hel} are ω surfaces, which are the most accurate continuous “density” surface approximations to describing neutral tangent planes with the residual slope errors being caused almost solely by neutral helicity (Klocker et al. 2009a,b).

The term e_{ω}^{hel} is studied on two different ω surfaces: $\omega = 27.25 \text{ kg m}^{-3}$ and $\omega = 27.75 \text{ kg m}^{-3}$ (Fig. 2). The average pressures of these surfaces are 1000 and 1800 dbar, respectively. These particular surfaces were chosen because both of these surfaces extend over most parts of the global ocean and cover quite different depth ranges. The results shown here are very similar on surfaces below and above these two surfaces. The highest values of e_{ω}^{hel} occur in the Southern Ocean, with large values also occurring close to the outcropping regions in the North Atlantic. Along most of the Antarctic Circumpolar Current (ACC), the magnitude of the diapycnal velocities is greater than 10^{-7} m s^{-1} . These velocities appear as both upward and downward diapycnal velocities. The regions of large e_{ω}^{hel} are created by neutral helicity forming from large isopycnal pressure gradients and isopycnal temperature gradients [see Eq. (2)] occurring near outcropping density surfaces. The main change we observe ongoing from a less dense surface to a denser one is that the regions of high e_{ω}^{hel} in the Southern Ocean are more confined to a thinner region on the less dense surfaces and are wider in the latitudinal direction on denser surfaces.

Another way of looking at the diapycnal advection caused by neutral helicity is to use zonal-mean values of e_{ω}^{hel} (averaged along ω surfaces). We consider the zonal

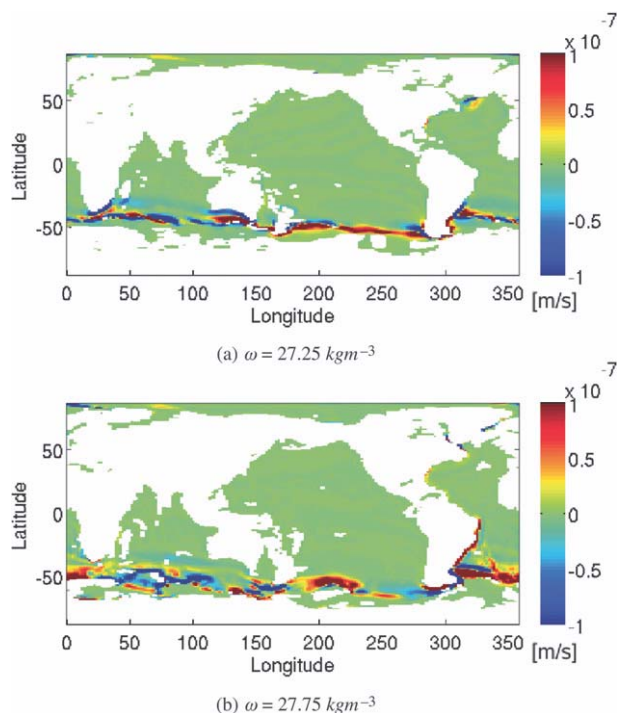


FIG. 2. Diapycnal advection due to neutral helicity e_{ω}^{hel} on (a) an $\omega = 27.25 \text{ kg m}^{-3}$ surface (with an average pressure of approximately 1000 dbar) and (b) an $\omega = 27.75 \text{ kg m}^{-3}$ surface (with an average pressure of approximately 1800 dbar). Red patches show an upward diapycnal velocity, and blue patches show a downward diapycnal velocity. The largest diapycnal velocities occur in the Southern Ocean and the North Atlantic, where the isopycnal gradients of pressure and conservative temperature and therefore neutral helicity are the largest.

mean of e_{ω}^{hel} over each of the Atlantic Ocean, Pacific Ocean, and Indian Ocean basins separately (Fig. 3). The southern Atlantic Ocean (Fig. 3a) has a positive (upward) e_{ω}^{hel} in the upper layers and negative (downward) e_{ω}^{hel} beneath. In contrast, the Pacific Ocean (Fig. 3b) shows positive values of e_{ω}^{hel} on the northern limit of the Antarctic Circumpolar Current and negative values of e_{ω}^{hel} on the ACC's southern extent. The Indian Ocean (Fig. 3c) is dominated by a negative e_{ω}^{hel} . Almost the entire diapycnal velocity caused by neutral helicity is in the Southern Ocean. The North Atlantic is the only other region where we can see large values of e_{ω}^{hel} . However, the e_{ω}^{hel} values in the North Atlantic are much smaller than in the Southern Ocean, and these values are confined to single grid cells instead of forming large patches of one sign.

To further understand the physics behind the diapycnal advection due to neutral helicity, we compare the zonal mean (averaged along ω surfaces) of e_{ω}^{hel} (Fig. 4a), the zonal mean of $gN^{-2}H^n$ (Fig. 4b), and the zonal mean of the slope errors s (Fig. 4c). Large values of e_{ω}^{hel} , $gN^{-2}H^n$,

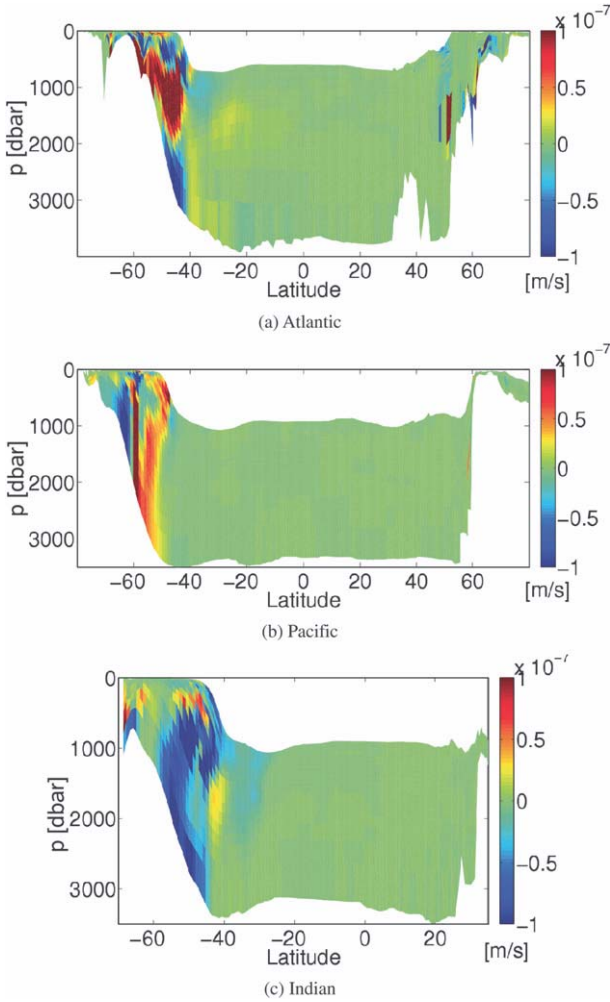


FIG. 3. Zonal mean of e_{ω}^{hel} along ω surfaces in (a) the Atlantic Ocean, (b) the Pacific Ocean, and (c) the Indian Ocean. Red patches show an upward zonal-mean diapycnal velocity, and blue patches show a downward zonal-mean diapycnal velocity.

and the slope errors tend to occur in similar locations, but the signs and shape of these values can be different. The difference between neutral helicity and the slope errors is probably due to the algorithm used to construct ω surfaces, redistributing the slope errors slightly differently than one might expect to minimize the slope errors over the global ocean. The slope errors and e_{ω}^{hel} show very similar patterns.

We have shown that neutral helicity causes e_{ω}^{hel} on the order of $O(10^{-7} \text{ m s}^{-1})$. In most regions with high values of e_{ω}^{hel} , patches of positive e_{ω}^{hel} occur with patches of negative e_{ω}^{hel} and vice versa. Hence, we explore whether there is a net diapycnal transport due to these velocities when integrated over the global ocean. We consider the transports through ω surfaces (Figs. 5, 6), σ_0 surfaces, and σ_2 surfaces (Fig. 6). The diapycnal transports through the

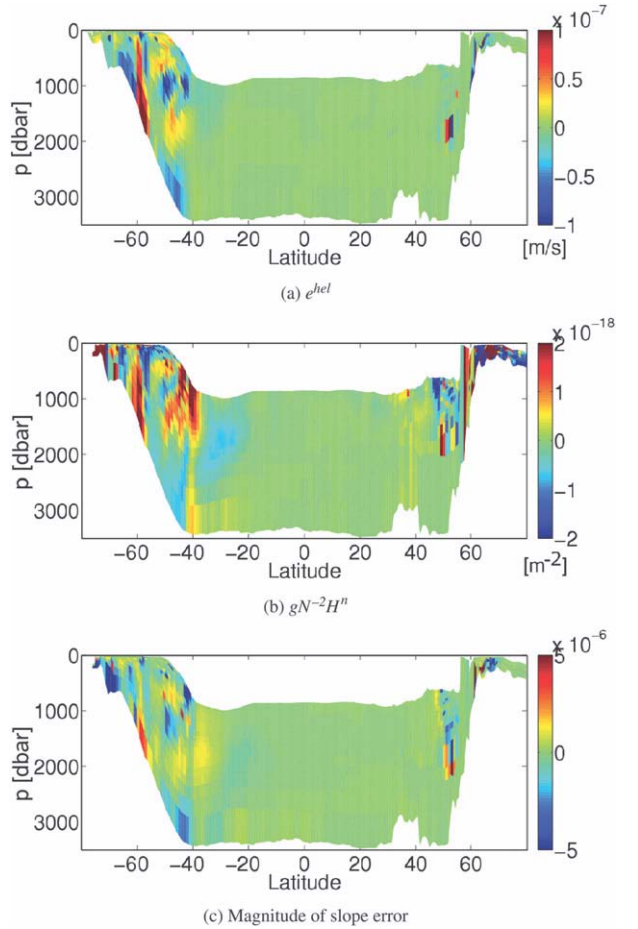


FIG. 4. Zonal mean along ω surfaces of (a) the diapycnal advection e_{ω}^{hel} , (b) $gN^{-2}H^n$, and (c) the slope error s .

ω surfaces in Fig. 5 (blue line) exclude data above the base of the mixed layer, a region where processes other than neutral physics are dominant. The transports excluding data above 200 dbar are also considered (black line) and do not always align with the blue line. This discrepancy is due to complicated processes in the shallow Southern Ocean. The algorithm used to construct ω surfaces encounters numerical issues near the base of the mixed layer; therefore, we get spikes in our transports, as can be seen when looking at the blue line in contrast to the black.

We now look at transports caused by e^{hel} through potential density surfaces (see Fig. 6). For all of the following calculations, data above 200 dbar are excluded. Figure 6 shows transports associated with $e_{\sigma_0}^{\text{hel}}$ to be much larger than the transports associated with e_{ω}^{hel} , with even the transports through σ_2 surfaces being approximately twice as large as those through ω surfaces. The diapycnal transport through the ω surfaces is almost solely due to neutral helicity.

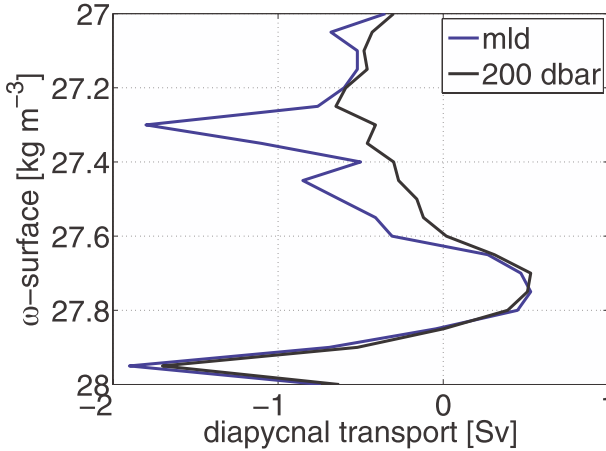


FIG. 5. A vertical profile of diapycnal transports caused by the diapycnal advection through ω surfaces. The blue line excludes data shallower than the mixed layer, and the black line excludes data shallower than 200 dbar. The spikes of the blue line are due to problems with the construction of ω surfaces close to the mixed layer.

The $e_{\sigma_0}^{\text{hel}}$ transports show a strong increase with depth. These larger $e_{\sigma_0}^{\text{hel}}$ transports occur because potential density surfaces are further away from being neutral than ω surfaces. The increase of the transports associated with e^{hel} with depth is due to the increasing pressure difference from the reference pressure. This can be understood by looking at the slope difference s between a potential density surface $\nabla_{\sigma} z$ and a neutral tangent plane $\nabla_n z$, which can be written as (McDougall 1988)

$$s = \nabla_n z - \nabla_{\sigma} z = -\frac{\nabla_n \Theta}{\Theta_z} (\mu - 1), \quad (13)$$

where μ is defined as

$$\mu = \frac{\beta^{\Theta}(p)}{\beta^{\Theta}(p_r)} \frac{r(R_p - 1)}{(R_p - r)}. \quad (14)$$

The stability ratio of the water column R_p and r are defined as

$$R_p = \frac{\alpha^{\Theta} \Theta_z}{\beta^{\Theta} S_z}; \quad r = \frac{\alpha^{\Theta}(p)/\beta^{\Theta}(p)}{\alpha^{\Theta}(p_r)/\beta^{\Theta}(p_r)}, \quad (15)$$

where p_r is the reference pressure. From Eq. (13), the slope of a potential density surface differs from the slope of a neutral tangent plane because of the temperature gradient along the neutral tangent plane. In the Southern Ocean, where this isopycnal temperature gradient is large and mainly of one sign, Eq. (13) implies a significant slope difference of one sign, as shown in the frequency distribution of slope errors for the ω surface and

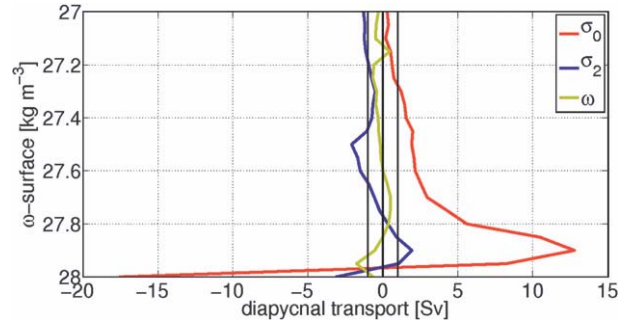


FIG. 6. A vertical profile of diapycnal transports caused by the diapycnal advection through ω surfaces, σ_0 surfaces, and σ_2 surfaces. The vertical black lines show 0 and ± 1 Sv. All data above 200 dbar are excluded.

the σ_0 surface in Fig. 7. In this figure, the slope errors on the potential density surface are larger than on the ω surface and biased toward positive slope errors giving an additional e^{hel} transport. Therefore, $e_{\sigma_0}^{\text{hel}}$ in this case is not only due to neutral helicity but also due to errors caused by the way potential density surfaces are defined.

Another reason for increased values of transports though σ_0 surfaces are issues concerning regions in which the vertical stratification of σ_0 decreases downward, which is also why σ_0 surfaces have not been routinely used as the vertical coordinate of density coordinate models for about a decade now (Sun et al. 1999). Therefore, diagnostic calculations of the diapycnal velocity, such as $e^a = (1/\sigma_0^a)(D\sigma^a/Dt)$, become ill defined where $(\sigma_0)_z = 0$. Therefore, $e_{\sigma_0}^{\text{hel}}$ in this case is not only due to neutral helicity but also due to errors caused by the way potential density surfaces are defined.

Diapycnal transports larger than e_{ω}^{hel} but much smaller than $e_{\sigma_0}^{\text{hel}}$ are caused by $e_{\sigma_2}^{\text{hel}}$. This is due to σ_2 surfaces being less neutral than ω surfaces; however, with its reference pressure chosen to optimize these potential density surfaces for the entire water column, they are a great improvement over σ_0 surfaces. Using a σ_2 surface also avoids issues with density inversions in the deep ocean, which causes a substantial part of $e_{\sigma_0}^{\text{hel}}$ in the deep ocean. Because of the minimization procedure used to construct ω surfaces (minimizing the slope error s), we expect e^{hel} to be caused by neutral helicity (in the case of an idealized ocean with zero neutral helicity, this minimization procedure used to construct ω surfaces creates a surface with no remaining slope errors).

The e_{ω}^{hel} transports are smaller than 1 Sv ($1 \text{ Sv} = 10^6 \text{ m}^3 \text{ s}^{-1}$) for most of the water column. These are small transports compared to those caused by other forms of water-mass transformation, such as bottom water production, cabbeling, or thermobaricity. However, even though the global integral of the e_{ω}^{hel} transports is not large,

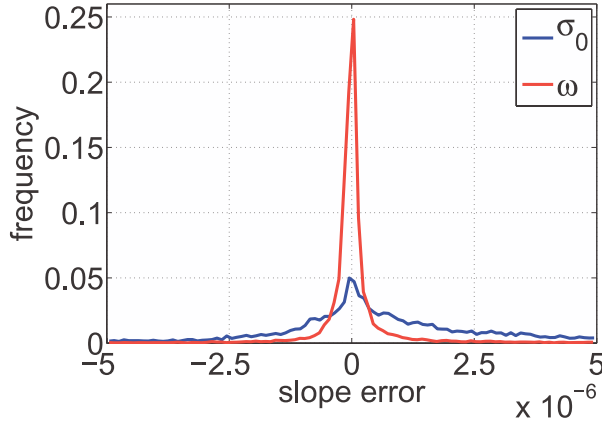


FIG. 7. The frequency distribution of the magnitude of slope errors s . Red is for an $\omega = 27.25 \text{ kg m}^{-3}$ surface, and blue is for a σ_0 surface with the same average pressure as the $\omega = 27.25 \text{ kg m}^{-3}$ surface. Note the biased distribution of the slope errors on the σ_0 surface.

the regional velocities caused by $e^{\text{hel}}_\omega [O(10^{-7} \text{ m s}^{-1})]$ are comparable to diapycnal velocities caused by cabbeling and thermobaricity, as quantified by McDougall (1987b).

From Fig. 2, we know that e^{hel} appears in positive and negative patches, which cancels much of the diapycnal transport shown in the previous figures. In Fig. 8, we therefore show e^{hel} for an ω surface, a σ_0 surface, and a σ_2 surface, all with an average pressure of 1200 dbar. This figure shows how going from a surface that is far away from being neutral (the σ_0 surface in Fig. 8a), to a surface that is closer to being neutral (the σ_2 surface in Fig. 8b), and to a surface that is as close as we can get to being neutral (the ω surface in Fig. 8c) the patches of e^{hel} reduce from large regions of the global ocean to regions where neutral helicity is large (e.g., along the ACC). In these regions of high neutral helicity, it will be impossible to avoid diapycnal transports resulting from e^{hel} . Further improvements to minimize e^{hel} might be made by changing weights in the algorithm used to construct ω surfaces to align the patches of slope errors more accurately with patches of increased neutral helicity, but it is impossible to achieve zero e^{hel} in an ocean with nonzero neutral helicity.

4. The ocean's adjustment toward small neutral helicity

In the last section, we quantified e^{hel} in today's ocean: that is, an ocean with small neutral helicity (McDougall and Jackett 2007). However, what happens if the ocean is perturbed from its state with small neutral helicity (i.e., its "skinny" state, occupying little volume in three-dimensional S – Θ – p space; McDougall and Jackett 2007)? Will it adjust back to this skinny state? Using

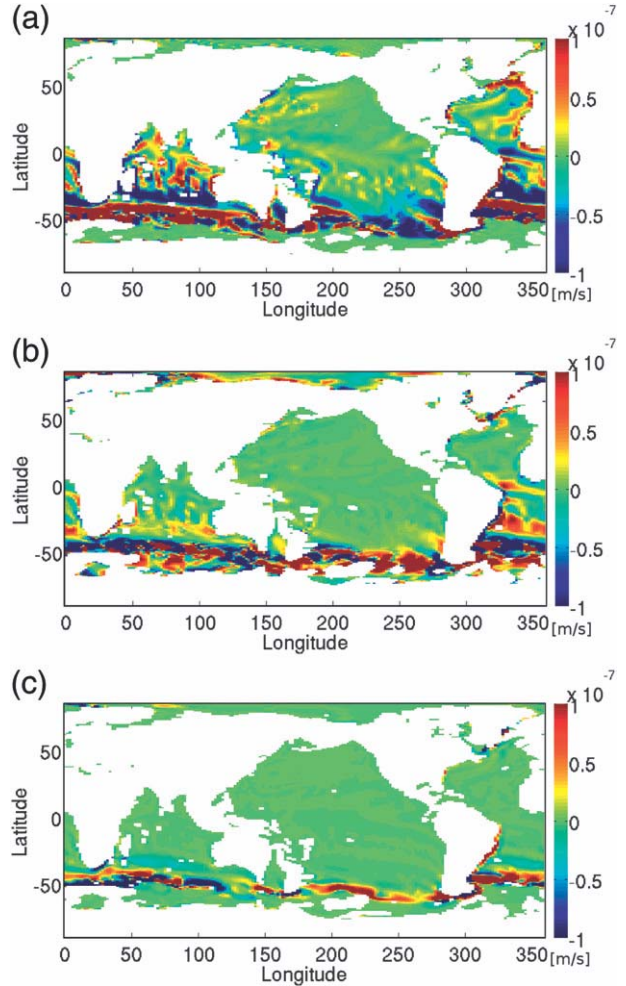


FIG. 8. (a) $e^{\text{hel}}_{\sigma_0}$ (b) $e^{\text{hel}}_{\sigma_2}$ and (c) e^{hel}_ω are shown on surfaces with an average pressure of 1200 dbar.

approximately neutral surfaces of any type, including those of Jackett and McDougall (1997), D. R. Jackett et al. (2009, unpublished manuscript), and Klocker et al. (2009a), for water-mass analysis essentially relies on neutral helicity being small in the ocean. Large neutral helicity would make the use of density surfaces for water-mass analysis impossible, causing large values of e^{hel} and D^f (Klocker et al. 2009a).

Here, we will perturb today's ocean to see how or if it adjusts back to a state with small neutral helicity. We therefore start with a model ocean that has small neutral helicity H^n : that is, small values of

$$\nabla_p S^0 \times \nabla_p \Theta^0 \cdot \mathbf{k}, \quad (16)$$

where Θ^0 and S^0 are the initial conservative temperature and salinity values. Now, we introduce the perturbation temperature $\Theta'(x)$ and $S'(x) = (a^\Theta/\beta^\Theta)(S, \Theta, p)\Theta'$. Here, the perturbation values only vary in the zonal direction.

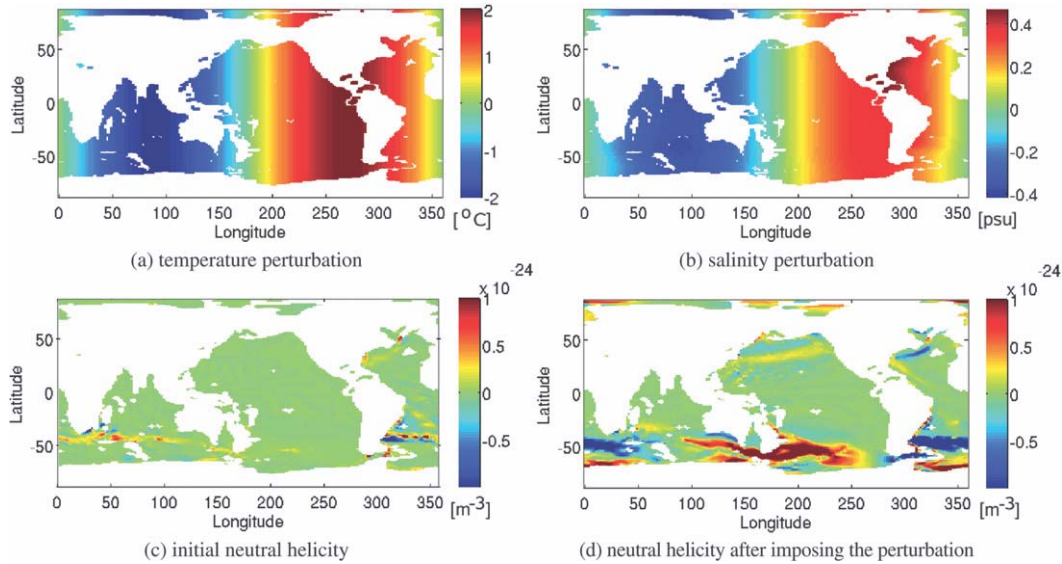


FIG. 9. (a) Θ , (b) S , and (c),(d) H^n perturbations on a pressure level of approximately 2400 dbar.

The perturbation conservative temperatures are chosen to vary zonally with the shape of a sine curve with a maximum temperature perturbation of 2°C with one cycle around the globe. The salinity perturbations are chosen to keep the density perturbations zero. These perturbations are shown in Figs. 9a,b.

Introducing these perturbations, we derive a quantity proportional to the perturbation neutral helicity,

$$\begin{aligned} \nabla_p(S^0 + S') \times \nabla_p(\Theta^0 + \Theta') \cdot \mathbf{k} &= \nabla_p S^0 \times \nabla_p \Theta^0 \cdot \mathbf{k} \\ &= \nabla_p S^0 \times \nabla_p \Theta' \cdot \mathbf{k} + \frac{\alpha^\Theta}{\beta^\Theta} \nabla_p \Theta' \times \nabla_p \Theta^0 \cdot \mathbf{k}, \\ &= \nabla_p \Theta' \times \left(-\nabla_p S^0 + \frac{\alpha^\Theta}{\beta^\Theta} \nabla_p \Theta^0 \right) \cdot \mathbf{k}. \end{aligned} \quad (17)$$

In this equation, the bracket in the last line would equal zero if $\nabla_p \rho^0 = 0$ (where ρ^0 is the initial density), in which case the perturbation neutral helicity $H^{n'}$ would be zero as well. The perturbation neutral helicity is therefore the largest in regions in which the gradient of density along isobars is at maximum, as is the case in the Southern Ocean. With the zonal perturbation of temperature and the meridional gradient of density along isobars in the Southern Ocean, $\nabla_p \Theta' \times \nabla_p \rho$ is large; therefore, the imposed perturbed neutral helicity is large. This can be seen in Fig. 9d, which shows high values of neutral helicity in the Southern Ocean with the maxima in regions where the gradients of the perturbation temperatures and salinities have their maxima.

In Fig. 10, a two-dimensional view of the hydrography is shown with salinity plotted against a linear combination

of conservative temperature and pressure of the Atlantic Ocean. Colors represent latitude, with blue in the south and red in the north. From McDougall and Jackett (2007), we know that the ocean would be represented on a single surface in $S-\Theta-p$ space if $H^n = 0$. In this figure, the panel representing the perturbed state (Fig. 10a) shows that the hydrography occupies a significant volume in this space, whereas the panel representing the original state (Fig. 10b) occupies significantly less volume and is therefore closer to being on a surface, which we would expect from an ocean with small H^n . This additional volume can be seen better when plotting the perturbed hydrography on a three-dimensional $S-\Theta-p$ diagram (not shown here) and rotating this diagram.

The evolution of neutral helicity after the perturbation is shown in Fig. 11, and its global root-mean-square values are shown in Fig. 12. These figures show how the enhanced values of neutral helicity caused by the perturbation of conservative temperatures and salinities decreases with time, reaching levels close to the initial ocean before the perturbation after approximately 50 yr. From Fig. 13, which shows the temperature difference of the evolving perturbed ocean and the initial ocean, it is apparent that, apart from the Southern Ocean, the temperature takes much longer to recover after the perturbation than neutral helicity. This is likely due to the increased isopycnal diffusion caused by the enhanced temperature and salinity gradients.

Changes in the diapycnal transports caused by nonlinearities in the equation of state of seawater (i.e., cabbeling, thermobaricity, and the diapycnal advection due to neutral helicity) can be seen in Fig. 14. These transports,

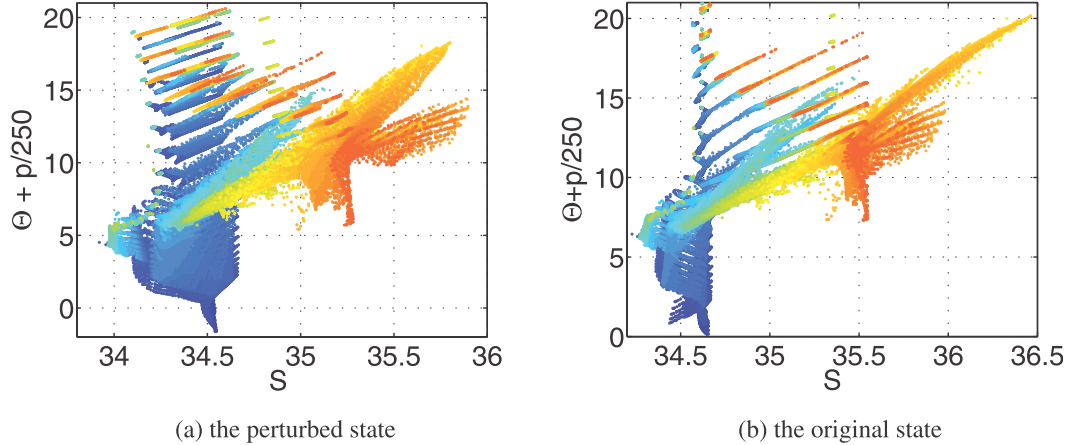


FIG. 10. A two-dimensional view of the Atlantic Ocean with salinity being plotted against a linear combination of conservative temperature and pressure: (a) perturbed and (b) initial state. Color represents latitude, with blue in the south and red in the north.

calculated on an $\omega = 27.75 \text{ kg m}^{-3}$ surface, rapidly increase to large values of up to almost 10 Sv quickly after the perturbation and decrease substantially after approximately 25 yr. Horizontal plots of these transports on the same ω surface are shown in Fig. 15. In these horizontal plots, one can see that, even though e_{ω}^{hel} is not the most dominant diapycnal advection when integrated globally compared to cabbeling and thermobaricity, locally it seems to be the most dominant form of diapycnal advection. The most important point to note here is the rapid adjustment of the ocean back to a state with small neutral helicity. Even though the perturbation used here is of unrealistically large magnitude, the ocean readjusts quickly and the slope errors and therefore e_{ω}^{hel} readjust back to very similar values as estimated for today's ocean.

5. Vertical advection caused by temporal changes in the ocean's hydrography

The diapycnal advection due to neutral helicity, as described in the last section, is due to the spatial variation of temperature and salinity in the ocean's hydrography. Here we will describe a similar process; however, in this case it is due to the temporal changes of salinity and temperature in the ocean. This vertical advection is what we call e^{tmp} . We look at the S - Θ - p values of one cast at a time and calculate the local direction of mixing (in pressure and time) between two realizations of the same cast separated in time by a month. We do this for each month of an annual cycle, beginning and finishing in January. The left side of Fig. 16 shows the Θ - p diagram of such a "seasonal" neutral trajectory. We know that the depth change around a closed loop (in this case in time) δz can also be calculated by (McDougall and Jackett 1988)

$$-\delta z N^2 g^{-1} \approx T_b^{\Theta} \oint_t p d\Theta. \quad (18)$$

The rhs of Eq. (18) is equal to the enclosed area in the Θ - p diagram in Fig. 16. In this figure, we can also see the difference in pressure between January of the first year and January of the second year (see the enlargement on the right of the Θ - p diagram). This process is physically similar to the helical nature of neutral trajectories (McDougall and Jackett 1988); however, instead of spatial variations of the ocean's hydrography, we are looking at its temporal variations [cf. Eqs. (18) and (A1)].

We construct an example of this depth change due to temporal changes (Fig. 17). As an initial condition, we chose S - Θ - p values on an ω surface with an average pressure of approximately 800 dbar. Most of this vertical velocity is confined to a narrow region along the Antarctic Circumpolar Current. Locally, the vertical velocities can exceed 10^{-7} m s^{-1} . Larger cohesive regions have vertical velocities around 10^{-8} m s^{-1} , cumulating as a downward vertical transport of approximately 0.1 Sv. This vertical velocity resulting from seasonal changes of hydrography is found to decrease with depth. Note that these vertical velocities are approximately one order of magnitude smaller than the diapycnal advection due to e^{hel} . These estimates of e^{tmp} assume the seasonal cycle of S - Θ - p values to be periodical; that is, the hydrography in the first year is the same as the hydrography of the following year. Aperiodic seasonal changes in the hydrography have not been looked at in this work and might change estimates of e^{tmp} . Additionally to the seasonal changes in hydrography, another source of temporal changes in the ocean is associated with mesoscale eddies, which has not been looked at here.

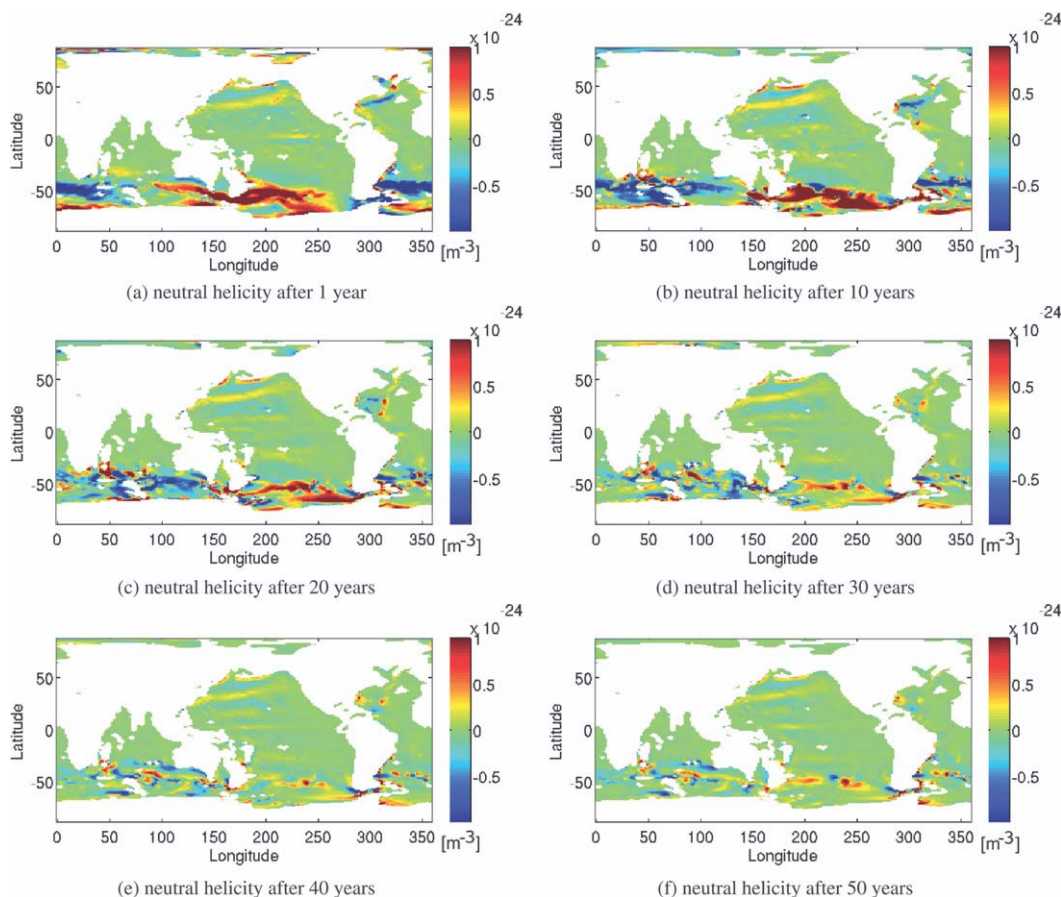


FIG. 11. Neutral helicity at certain times after the perturbation are shown on a pressure level of 2400 dbar: (a)–(f) after 1 to 50 yr.

6. Summary and conclusions

We have derived a “density” conservation equation with respect to continuous “density” surfaces, showing that two “extra” processes have to be accounted for when using continuous “density” surfaces as a reference frame instead of neutral tangent planes. These processes are the diapycnal advection due to neutral helicity e^{hel} and the vertical advection due to the temporal variation of the ocean’s hydrography e^{tmp} . Using continuous “density” surfaces as the reference frame for water-mass analysis has been common for quite some time, but the two extra processes described here have been ignored.

Using the output of a numerical ocean model, we have quantified the diapycnal advection e^{hel} caused by the ill-defined nature of neutral surfaces. This diapycnal advection arises as a result of using continuous “density” surfaces as a framework for viewing ocean circulation. If the equation of state of seawater were linear, this approach would be correct and diapycnal flow would only occur as a result of the usual well-understood mixing such as small-scale turbulent mixing and double-diffusive

convection. Because the equation of state is nonlinear and the neutral helicity H'' is nonzero in the ocean, we have to deal with the helical nature of neutral trajectories (McDougall and Jackett 1988), which means that, depending on the path a neutral trajectory takes, it will end up at some distance above or below a continuous “density” surface. This effect therefore always produces

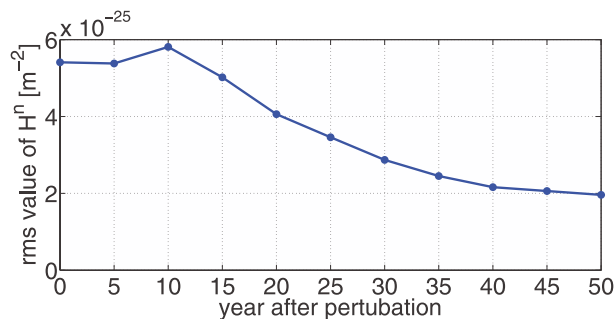


FIG. 12. The evolution of neutral helicity at the 2500-dbar isobar from the time of perturbation until 50 yr after.

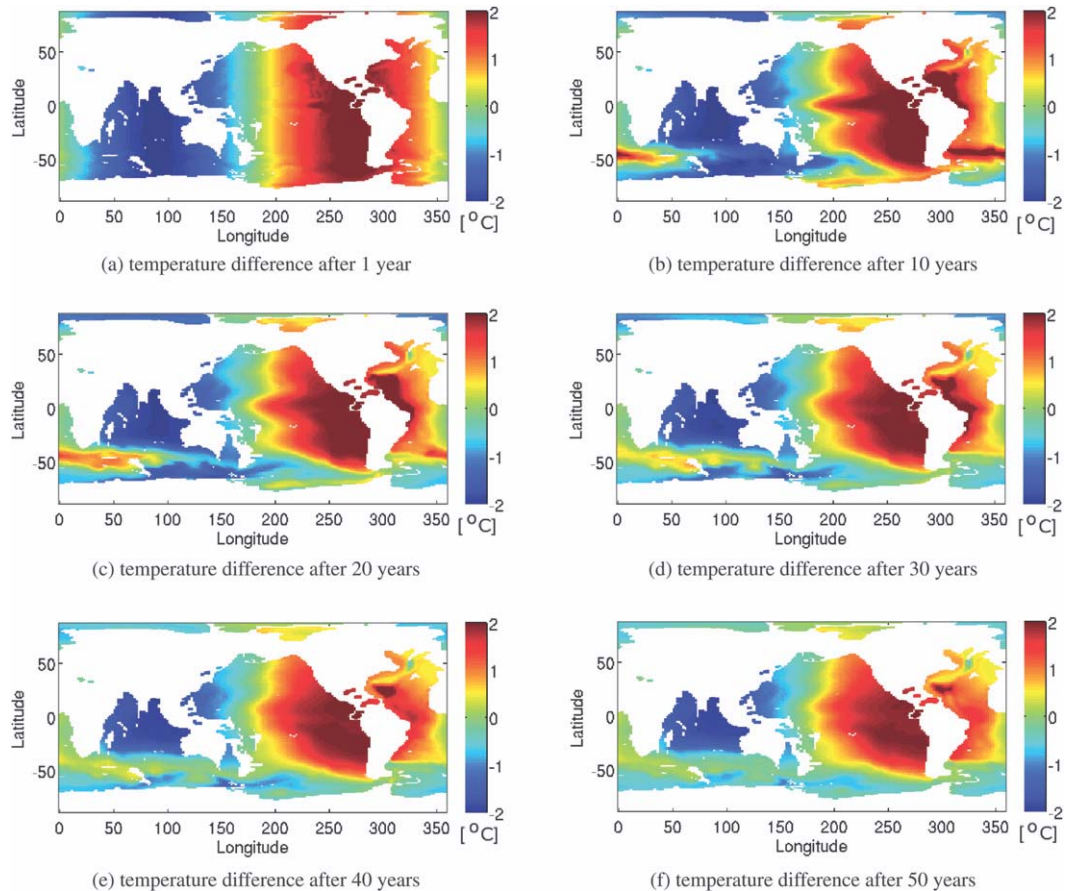


FIG. 13. Temperature changes from the ocean after the perturbation are shown on a pressure level of 2400 dbar: (a)–(f) after 1 to 50 yr.

diapycnal advection, no matter which density surface we use. It is not possible to quantify this diapycnal advection in a climatology because of the lack of lateral velocities, but McDougall and Jackett (2007) have shown that neutral helicity is small in a climatology, which gives us confidence that this diapycnal advection is small in these datasets as well.

In this work, we show that this diapycnal velocity e^{hel} can be on the order of 10^{-7} m s^{-1} . The highest values of e^{hel} occur in the Southern Ocean and in the North Atlantic. In these regions, e^{hel} is of a similar order of magnitude to diapycnal velocities caused by small-scale turbulent mixing and also by cabbeling and thermobaricity, which have been quantified by McDougall (1987b) and in this paper. This means that, when one is interested in quantifying water-mass transformation processes, such as cabbeling, thermobaricity, or small-scale turbulent mixing, it is important to take e^{hel} into account.

The regions of substantial e^{hel} are observed to correspond closely to regions where neutral helicity, $H^n = g^{-1} N^2 T_b^\Theta \nabla_a p \times \nabla_a \Theta \cdot \mathbf{k}$, is high. Most regions of the global ocean seem to have adjusted in a way to attain

small values of neutral helicity (McDougall and Jackett 2007). The main exception seems to be the outcropping regions: that is, the regions where the atmosphere has a chance to modify deep water masses. This atmospheric

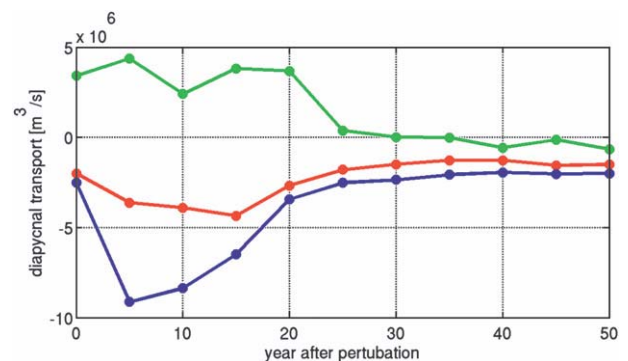


FIG. 14. The transports caused by nonlinearities in the equation of state of seawater are shown from the time of the Θ and S perturbation until 50 yr after on an $\omega = 27.75 \text{ kg m}^{-3}$ surface. The blue line shows transports due to cabbeling e^{cab} , the red line shows transports due to thermobaricity e^{therm} , and the green line shows transports due to neutral helicity e^{hel} .

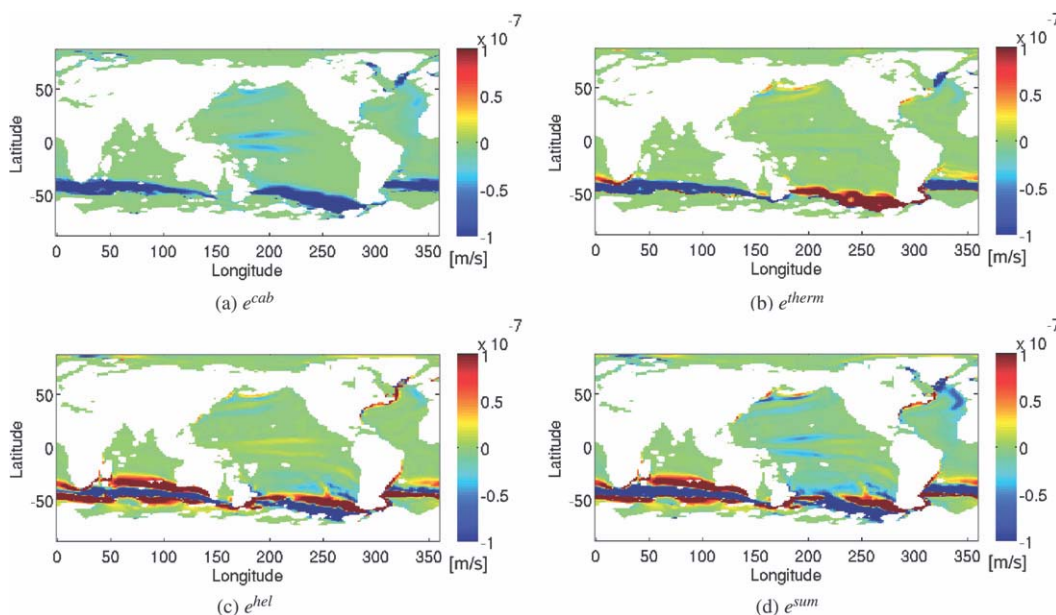


FIG. 15. Diapycnal velocities due to nonlinearities in the equation of state of seawater are shown 5 yr after the perturbation of Θ and S on an $\omega = 27.75 \text{ kg m}^{-3}$ surface. These are (a) e^{cab} , the diapycnal velocity due to cabelling; (b) e^{therm} , the diapycnal velocity due to thermobaricity; (c) e^{hel} , the diapycnal velocity due to neutral helicity; and (d) the sum of these three diapycnal velocities.

modification could act as a perturbation of the ocean from a state with very small neutral helicity.

We find that net global diapycnal transports due to e_{ω}^{hel} are less than 1 Sv on most ω surfaces. Regionally, this transport can be either upward or downward. Therefore,

even though in certain regions the diapycnal advection due to neutral helicity can be significant, the globally integrated transports remain relatively small. To understand what happens if we use less accurate density surfaces for our calculations for e^{hel} , we repeated the

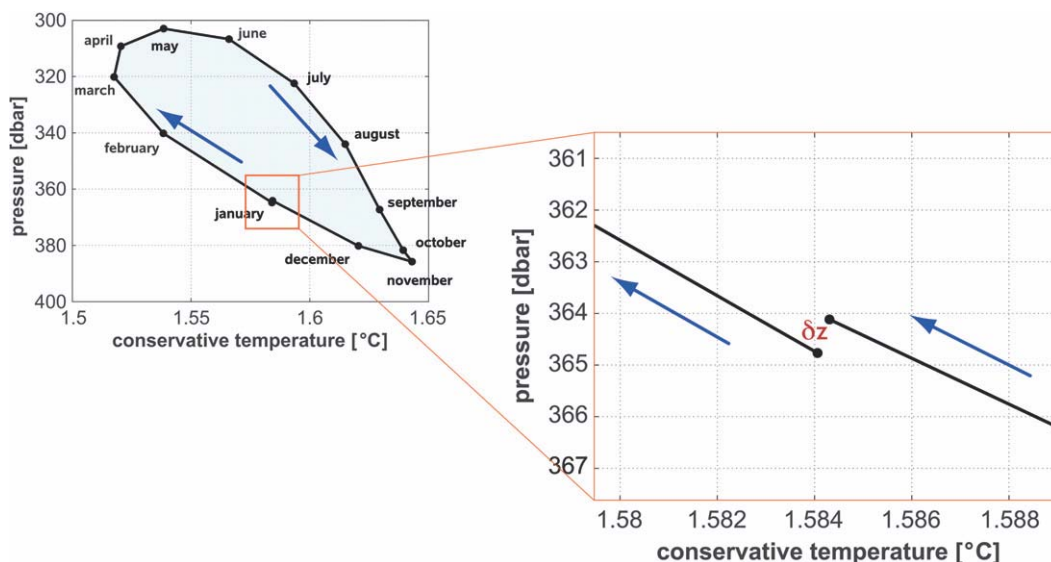


FIG. 16. A Θ - p diagram showing the seasonal changes following a neutral “trajectory” throughout one year on one single cast in space. One can see that the loop in this diagram is almost closed. The gap at the end (January, which is shown magnified on the right) is the depth change δz of the neutral trajectory through time. This depth change can be calculated via $-\delta z N^2 g^{-1} \approx T_b^{\Theta} \oint p d\Theta$ (McDougall and Jackett 1988).

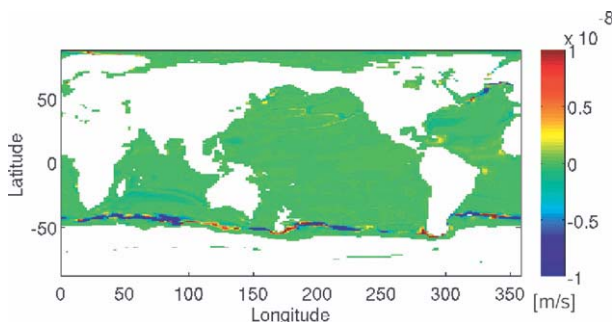


FIG. 17. The vertical advection due to temporal changes in the ocean's hydrography. Initial S – Θ – p values are chosen on an $\omega = 27.25 \text{ kg m}^{-3}$ surface that has an average pressure of approximately 800 dbar.

same procedure as earlier to derive transports through σ_0 surfaces and σ_2 surfaces: that is, transports associated with $e_{\sigma_0}^{\text{hel}}$ and $e_{\sigma_2}^{\text{hel}}$. This analysis for potential density surfaces resulted in transports twice as large (for σ_2) or larger (for σ_0) than through ω surfaces. Therefore, using inaccurate density surfaces can lead to very large “fictitious” diapycnal transports. We call these transports fictitious because using these inaccurate density surfaces leads to e^{hel} not only being due to neutral helicity but also due to errors made when defining density surfaces.

We have also conducted a perturbation experiment with a numerical ocean model in which we perturb today's ocean into a state in which it has enhanced values of neutral helicity. These enhanced values of neutral helicity cause an increase in thermobaricity, cabbeling, and e_{ω}^{hel} in the years following the perturbation and decrease to values close to the ones before the perturbation after approximately 50 yr. This shows that the ocean adjusts rapidly toward a state with small neutral helicity.

We also demonstrated how seasonal changes in the ocean's hydrography can cause vertical advection. This vertical advection e^{imp} is on $O(10^{-8} \text{ m s}^{-1})$ (i.e., an order of magnitude less than the diapycnal advection due to e^{hel}) and causes a net global downward diapycnal transport of approximately 0.1 Sv. This form of vertical advection is therefore relatively insignificant as a water-mass transformation mechanism.

Acknowledgments. We thank Jaci Brown for helping to improve the readability of this manuscript. We also thank two anonymous reviewers for valuable comments on the manuscript. The first author is supported by a joint CSIRO-UTAS Ph.D. scholarship in Quantitative Marine Science (QMS) and a top-up CSIRO Ph.D. stipend (funded from Wealth from Oceans National Research Flagship). This research was supported by the Antarctic Climate and Ecosystems Cooperative Research Centre

(ACE CRC) and also contributes to the CSIRO Climate Change Research Program.

APPENDIX

Alternative Ways of Calculating Diapycnal Motion due to Neutral Helicity

In this work, we quantify the diapycnal velocity due to neutral helicity e^{hel} . Therefore, after finding an approximately neutral surface, we have to calculate the residual slope error \mathbf{s} and the lateral velocity \mathbf{V} on this surface. Then, we can calculate e^{hel} everywhere on this surface, including the transports it causes. We have shown in this paper that it is necessary to use accurate approximately neutral surfaces. If we use other density surfaces that do not minimize the residual slope error \mathbf{s} , some of this error is not due to neutral helicity but due to errors associated with defining, for example, a potential density surface. This problem can be seen in the frequency distribution of slope errors in an ω surface and a potential density surface in Fig. 7. The errors on the potential density surface are larger and unevenly distributed, leading to a larger transport through this surface.

Instead of calculating e^{hel} at every point on an approximately neutral surface, one can follow a neutral trajectory around the ocean and quantify its vertical displacement from this surface. McDougall and Jackett (1988) described the vertical displacement of a neutral trajectory from an approximately neutral surface with the equation

$$-\delta z N^2 g^{-1} \approx \oint \boldsymbol{\epsilon} \cdot d\mathbf{l} = T_b^\Theta \oint p d\Theta. \quad (\text{A1})$$

Here, they relate the depth change δz of a neutral trajectory after doing a closed loop in x – y space in the ocean to a closed line integral of the density gradient error $\boldsymbol{\epsilon}$ on an approximately neutral surface A . McDougall and Jackett (1988) argued that, no matter which density surface is used, the depth change δz will be unchanged. They assumed that, by using different density surfaces, one changes the local slope error, but when calculating the closed line integral around the circular path these large positive and negative slope errors would cancel.

This argument is based on two assumptions:

- The flow is circular; that is, the mean flow always comes back to its original horizontal position, even though its depth might be different.
- The lateral velocity on an approximately neutral surface is equal to the lateral velocity along a whole loop of a circular trajectory.

The first point assuming circular flow is definitely not true in the real ocean, because the pathways of the mean flow are more complicated and usually do not come back to their original horizontal position.

The second assumption assumes the lateral velocity to be constant with depth. In the real ocean, the lateral velocity can change quickly with depth and therefore this assumption is only valid if the approximately neutral surface is a very close approximation to the neutral tangent planes.

We prefer to not make these two assumptions, so we calculate e^{hel} as described in this paper instead of using this technique. For both techniques, we need accurate approximately neutral surfaces; however, because of calculating e^{hel} on every point on an approximately surface, we avoid having to deal with the two assumptions described here. It would also be more complicated to calculate diapycnal transports from vertical displacement of neutral trajectories than from local values for e^{hel} .

REFERENCES

- Bryan, K., and L. J. Lewis, 1979: A water mass model of the world ocean. *J. Geophys. Res.*, **84**, 2503–2517.
- Griffies, S. M., M. J. Harrison, R. C. Pacanowski, and A. Rosati, 2004: A technical guide to MOM4. NOAA/GFDL Ocean Group Tech. Rep. 5, 342 pp.
- Ivers, W. D., 1975: The deep circulation in the northern North Atlantic with special reference to the Labrador Sea. Ph.D. thesis, University of California, San Diego, 179 pp.
- Jackett, D. R., and T. J. McDougall, 1997: A neutral density variable for the world's oceans. *J. Phys. Oceanogr.*, **27**, 237–263.
- Klocker, A., and T. J. McDougall, 2010: Influence of the nonlinear equation of state on global estimates of diapycnal advection and diffusion. *J. Phys. Oceanogr.*, **40**, 1690–1709.
- , —, and D. R. Jackett, 2009a: A new method for forming approximately neutral surfaces. *Ocean Sci.*, **5**, 155–172.
- , —, and —, 2009b: Corrigendum to “A new method for forming approximately neutral surfaces” published in *Ocean Sci.*, **5**, 155–172, 2009. *Ocean Sci.*, **5**, 191.
- McDougall, T. J., 1987a: Neutral surfaces. *J. Phys. Oceanogr.*, **17**, 1950–1964.
- , 1987b: Thermobaricity, cabbeling, and water-mass conversion. *J. Geophys. Res.*, **92**, 5448–5464.
- , 1987c: The vertical motion of submesoscale coherent vortices across neutral surfaces. *J. Phys. Oceanogr.*, **17**, 2334–2342.
- , 1988: Neutral-surface potential vorticity. *Prog. Oceanogr.*, **20**, 185–221.
- , 2003: Potential enthalpy: A conservative oceanic variable for evaluating heat content and heat fluxes. *J. Phys. Oceanogr.*, **33**, 945–963.
- , and D. R. Jackett, 1988: On the helical nature of neutral trajectories in the ocean. *Prog. Oceanogr.*, **20**, 153–183.
- , and —, 2007: The thinness of the ocean in S – θ – p space and the implications for mean diapycnal advection. *J. Phys. Oceanogr.*, **37**, 1714–1732.
- , —, D. G. Wright, and R. Feistel, 2003: Accurate and computationally efficient algorithms for potential temperature and density of seawater. *J. Atmos. Oceanic Technol.*, **20**, 730–741.
- Reid, J. L., and R. J. Lynn, 1971: On the influence of the Norwegian–Greenland and Weddell Seas upon the bottom waters of the Indian and Pacific Oceans. *Deep-Sea Res.*, **18**, 1063–1088.
- Sun, S., R. Bleck, C. Rooth, J. Dukowicz, E. Chassignet, and P. Killworth, 1999: Inclusion of thermobaricity in isopycnal-coordinate ocean models. *J. Phys. Oceanogr.*, **29**, 2719–2729.
- Theodorou, A. J., 1991: Some considerations on neutral surface analysis. *Oceanol. Acta*, **14**, 205–222.